Research Article | Vol. 26, No. 16 | 6 Aug 2018 | OPTICS EXPRESS 21108
Optics EXPRESS

Investigation about the influence of longitudinal-mode structure of the laser on the relative intensity noise properties

YONGRUI GUO,[1] HUADONG LU,[1,2,*] MINZHI XU,[1] JING SU,[1,2] AND KUNCHI PENG[1,2]

[1] *State Key Laboratory of Quantum Optics and Quantum Optics Devices, Institute of Opto-Electronics, Shanxi University, Taiyuan 030006, China*
[2] *Collaborative Innovation Center of Extreme Optics, Shanxi University, Taiyuan, Shanxi 030006, China*
[*] *luhuadong@sxu.edu.cn*

Abstract: The influence of the longitudinal-mode structure (LMS) of the laser on the relative intensity noise (RIN) properties was investigated in this paper after an all-solid-state continuous-wave (CW) single-frequency 1064 nm laser with output power of 50.3 W was achieved. The LMS of the laser was manipulated by controlling the temperature of the nonlinear lithium triborate (LBO) crystal deliberately introduced to the resonator. When the laser worked with single-longitudinal-mode (SLM) operation, the stable RIN spectrum was observed and measured. Moreover, with the decrease of the nonlinear conversion efficiency (NCE), the frequency and amplitude of the resonant-relaxation oscillation (RRO) peak regularly shifted to the higher frequencies and increased, respectively. However, with further decrease of the NCE, the laser began to work with the multi-longitudinal-mode (MLM) or mode-hopping operation and the unstable RIN spectra of the laser were both observed not only at low frequencies but also at high frequencies. Once the NCE was moved away, the MLM or mode-hopping can only enhance the fluctuation of the laser RIN spectrum at the low frequencies (lower than the frequency of RRO). The experimental results directly revealed the relationship between the LMS of the laser and the RIN spectra, and confirmed definitely that the key to achieve a stable high power laser with low intensity noise was to realize single-frequency operation of the laser with free MLM and mode-hopping.

1. Introduction

High power all-solid-state continuous-wave (CW) single-frequency lasers are being paid attentions in lots of cutting-edge scientific research fields such as quantum network [1, 2], atom trapping and cooling [3], high-precision measurements [4] and so on, owing to their intrinsic advantages including narrow linewidth, low intensity noise in conjunction with high long-term stability. Specifically in the high precision measurements of weak signals, for instance gravitation-wave (GW) detections, the fluctuation of the laser intensity can couple the excess noise into the detected GW signal, which will make it rather difficult to distinguish the GW signal from the noise background of interferometer [5]. One way to overcome this issue is adopting a high power coherent light with fluctuations at the quantum noise limit (QNL) [6, 7], even a squeezed light with fluctuation below QNL in the detection systems [8, 9]. However, it is disappointing that the high output power laser is often accompanied with the high intensity noise, which is caused by the strong mode-hopping because of the mode competition [10]. So, it is important to investigate the influence of the mode-hopping on laser relative intensity noise (RIN) properties. So far, the most popular theory used to describe the intensity noise of a laser is quantum-mechanical intensity-noise transfer function developed by Ralph and Harb in 1996 [11]. The function can well depict the contribution of every noise source on the intensity noise of the laser. Based on the presented theory, the intensity noise of an injection-locked CW

#331540 https://doi.org/10.1364/OE.26.021108
Journal © 2018 Received 14 May 2018; revised 16 Jul 2018; accepted 19 Jul 2018; published 1 Aug 2018

Optics EXPRESS

Nd:YAG non-planar ring-oscillator laser was successfully investigated [12]. Subsequently, the influences of the transverse-mode [13] and longitudinal-mode [14] characteristics as well as the wavelength and frequency drift of the pump source [13] on the intensity noise of the laser were also experimentally analyzed. In 2000, Zhang *et al*. extended the intensity-noise transfer function to the laser diode pumped CW single-frequency-doubling lasers [15], and our group further extended this theory to investigation on the intensity noise of the laser with dual-wavelength output [16]. Besides, various methods were developed to suppress the intensity noise of the laser. Electronic negative feedback controllers acting as a noise eater have been commonly utilized to suppress intensity noise of the single-frequency laser around resonant-relaxation oscillation (RRO) frequencies [17–23]. Recently, the intensity noise of the laser at the low frequency near the RRO peak was also manipulated and suppressed by deliberately introducing an extra nonlinear loss to the laser resonator for modifying the dynamical behavior of the laser [16, 24, 25]. The intensity noises of the single-frequency lasers at high frequency can be significantly suppressed by using a mode-cleaner with high finesses [26–28]. The injection-locking stabilization scheme implemented by locking the frequency of the slave laser to a low power master oscillator with good noise performance is commonly employed to realize a high power single-frequency laser with low intensity noise [29–36]. However, the complicated construction directly limits their applications in various fields. Another way to obtain a high power single-frequency laser is designing a suitable and compact resonator which can directly realize high power output and low intensity noise. In this case, the incident pump power of the single-frequency laser can reach up to hundred-watt-level, the mode-hopping of the laser may be enhanced due to an enhanced beating between the lasing mode and non-lasing adjacent longitudinal modes for a high optical gain [37]. Furthermore, the fluctuation of RRO peak driven by vacuum fluctuations, dipole fluctuations and intra-cavity losses [11, 12] can be heightened significantly due to the interplay between the population inversion and the intra-cavity photons [24]. As a consequence, the laser performance including output power, longitudinal-mode structure (LMS) as well as intensity noise will be affected. Therefore, a good understanding of the impact of mode-hopping on the RIN properties is imperative in a high power single-frequency laser.

In this paper, an all-solid-state high power single-frequency 1064 nm laser was designed and constructed, and the influence of the LMS on the RIN spectrum of the 1064 nm laser was investigated. The LMS manipulation was implemented by controlling the deliberately introduced nonlinear loss. By recording the LMS of the laser and measuring the corresponding RIN spectrum, the influence of the LMS on the RIN spectrum of the laser was studied.

2. Experimental setup

The schematic diagram of the experimental setup was shown in Fig. 1. An all-solid-state single-frequency CW Nd:YVO_4 laser with figure-eight-shaped construct was firstly designed and built. The pumping source was a fiber-coupled laser diode (LIMO110-F400-DL-888-EX2040, LIMO co., Ltd.) with a center wavelength of 888 nm and a maximum output power of 120 W. Compared to the traditional pump wavelength of 808 nm, the visible advantages of the 888 nm laser as the pump source were the lower quantum defect and isotropic absorption, which can directly reduce the waste heat and allow the laser to operate with high output power and perfect beam quality [38–41]. The diameter and numerical aperture of the coupling fiber were 400 μm and 0.22, respectively. The pump radiation was focused into the gain medium by two lenses with the focal lengths of 30 mm and 80 mm, respectively. The input coupler M_1 was a concave-convex lens (R=1500 mm) coated with high transmissivity (HT) films at 888 nm (T_{888nm} > 99.5%) and high reflection (HR) films at 1064 nm (R_{1064nm} > 99.7%). M_2 was a plane-convex mirror (R=1500 mm) coated with HR films at 1064 nm (R_{1064nm} > 99.7%). M_3 and M_4 are two plane-concave mirrors both with curvature radius of 100 mm (R=-100 mm). M_3 was coated with HR films at 1064 nm (R_{1064nm} > 99.7%). The output coupler M_4 was coated with partial

Optics EXPRESS

transmission at 1064 nm and HT at 532 nm ($T_{532nm} > 95\%$). The gain medium was an α-cut composite YVO_4/Nd:YVO_4 rod (3 mm× 3 mm × (3+20) mm), including an un-doped end cap of 3 mm and Nd-doped part of 20 mm with concentration of 0.8% and a wedge angle of 1.5 degree at the second end face to keep stable polarization [42]. The front end-face of the Nd:YVO_4 crystal was coated with anti-reflection (AR) films at 1064 and 888 nm ($R_{1064nm;888nm} < 0.25\%$), and the second end-face was coated with AR films at 1064 nm ($R_{1064nm} < 0.25\%$). An optical diode comprised of an 8 mm long terbium gallium garnet crystal and a half-wave plate (HWP_1) was applied to eliminate the spatial hole burning effect and realize the unidirectional operation of the laser [43, 44]. A type-I non-critically phase-matched lithium triborate (LBO) crystal [45] (S_1, S_2: $AR_{1064nm;532nm}$) with a dimensions of 3 mm× 3 mm× 18 mm was deliberately inserted into the resonator to introduce the intra-cavity nonlinear loss [46, 47]. The LBO crystal was placed at the beam waist between M_3 and M_4, and the temperature of which was controlled by a homemade temperature-controller with the precision of 0.01 °C.

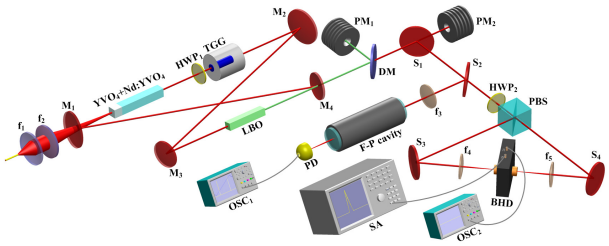

Fig. 1. Schematic diagram of the experimental setup. HWP_1, HWP_2, half-wave plate; TGG, terbium gallium garnet; LBO, lithium triborate; DM, dichroic mirror; S_1-S_4, beam splitter; PM_1, PM_2, power meter; PBS, polarization beam splitter; PD, photodetector; BHD, balanced homodyne detector; SA, spectrum analyzer; OSC_1, OSC_2, digitizing oscilloscope.

The output second-harmonic-wave (SHW) was separated from the fundamental-wave (FW) by a dichroic mirror and monitored by a power meter (PM_1) (LabMax-Top, Coherent). The main part of the FW laser leaked from S_1 was detected by another power meter (PM_2) (LabMax-Top, Coherent). A small part of the FW laser reflected by S_1 and S_2 was injected into a scanned confocal Fabry-Perot (F-P) cavity to monitor the LMS of the laser. The free spectrum range and finesse of the F-P cavity were 375 MHz and 200, respectively. The transmitted signal from F-P cavity was detected by a photodetector and the transformed signal was displayed on a digitizing oscilloscope (OSC_1: MSO 5204B, Tektronix). The leaked part from S_2 was equally divided into two parts by a 50/50 beam splitter composed of HWP_2 and polarization beam splitter and reflected by S_3 and S_4 and focused by f_4 and f_5 into a homemade balanced homodyne detector (BHD) to measure the RIN spectrum of the laser. The employed BHD was composed of two InGaAs photodiodes (ETX500, JDSU Corporation) in a single electronic board. The achieved common mode rejection ratio of the BHD was 60 dB and high enough to accurately calibrate the QNL [48]. The DC (direct current) output of the BHD was connected with the digitizing oscilloscope OSC_2 (TBS 1022, Tektronix) to monitor whether the light is totally received by each photodiode, the AC (alternating current) output was connected with a spectrum analyzer (N9320A, Agilent) to read the intensity noise spectrum of the laser, respectively.

3. Experimental results and analyses

In the experiment, based on the accurate measurement method of the intra-cavity linear loss of lasers by means of a nonlinear loss deliberately introduced to the laser resonator [49], the transmission of the output coupler was optimized and output coupler M_4 employed in the experiment was coated with the transmission of T_{1064nm}=25%. When the LBO crystal was

Optics EXPRESS

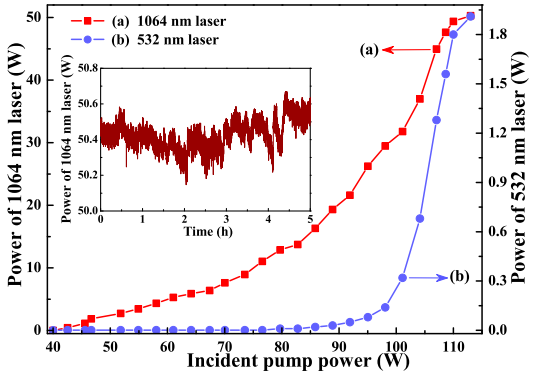

Fig. 2. Output power of 1064 nm laser (a) and 532 nm laser (b) versus incident pump power. Inset shows power stability during 5 h.

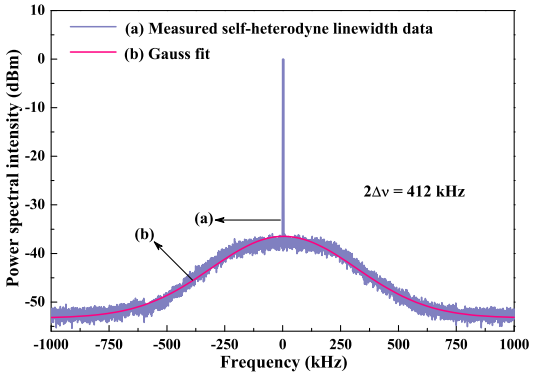

Fig. 3. Measured self-heterodyne linewidth data (a) with 25 km delay fiber and the Gaussian function fitting result (b) of 1064 nm laser.

working at the optimal phase-matching temperature of 149.0 °C, a stable single-frequency CW 1064 nm laser with the output power of 50.3 W was achieved under the pump power of 113 W. To the best of our knowledge, it was the highest output power single-frequency all-solid-state CW 1064 nm laser in a single resonator without any amplifiers. The output powers as a function of incident pump power were recorded in Fig. 2. It was depicted that a single-frequency 532 nm laser beam with the maximal output power of 1.91 W was simultaneously generated because of the existence of the LBO crystal. The corresponding optical-optical conversion efficiency was 46.20%. The beam quality M^2 was measured by a M^2 meter (M2SET-VIS, Thorlabs) and the measured values of M_x^2 and M_y^2 are 1.08 and 1.10, respectively. The measured degree of polarization of 1064 nm laser at the maximum output power was more than 110:1. The long-term power stability of 1064 nm laser was measured (Fig. 2 inset) and the peak-to-peak power fluctuations was less than ±0.50% during 5 h. The linewidth of the single-frequency 1064 nm laser was also measured by means of a delayed self-heterodyne interferometer [50]. The path length imbalance of 25 km between the long and short branches of the employed interferometer was long enough to measure the linewidth of the 1064 nm laser. A small part of 1064 nm laser was firstly divided into two equal parts by a polarization maintaining coupler and separately injected into two branches of the interferometer. Then the transmitted 1064 nm laser from two branches were combined in another polarization-maintaining coupler and the beat signal was directly detected by a fast detector (S/N29637, Thorlabs). Lastly, the detected signals was

Optics EXPRESS

recorded and analyzed by another spectrum analyzer. In the process of linewidth measurement, to avoid the $1/f$ noise of detection circuits, a polarization maintaining fiber-coupled acousto-optic modulator (T-M150-0.4C2G-3-F2P, Gooch & Housego) was utilized in the short branch to shift the beatings by 150 MHz from the baseband. The measured self-heterodyne linewidth data (shown as line (a) in Fig. 3) was fitted by the Gaussian lineshape function, and the fitted result was shown in curve (b) in Fig. 3. It was clear that the measured spectral linewidth of 1064 nm laser was 206 kHz.

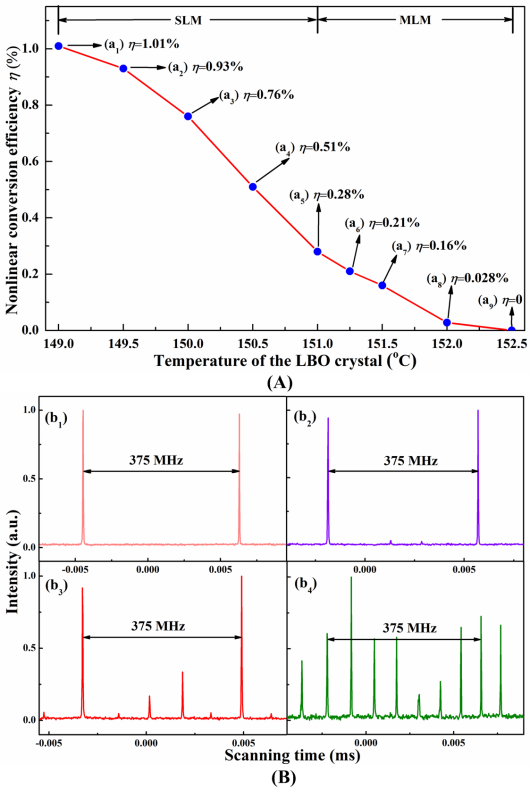

Fig. 4. The LMS of the laser with different operation conditions. (A), the NCE η as a function of the temperature of the LBO crystal, (a_1)~(a_9) recorded the NCE η with respect to the temperature of the LBO crystal at 149.0 °C~152.5 °C, respectively. (B), the LMS of the laser with respect to different NCE η. Curve (b_1), the LMS of the single-frequency laser with NCE $\eta \geq 0.28\%$; curve (b_2), the initial LMS of the laser with NCE $\eta = 0.21\%$, which would gradually evolve into the curve (b_3); when the NCE η of the laser was 0.16%, the LMS of the laser rapidly alternated between the curve (b_3) and curve (b_4); curve (b_4), the LMS of the laser with NCE $\eta = 0.028\%$; when the NCE η of the laser was zero, the LMS of the laser randomly switched between curves of (b_1), (b_2), and (b_3).

The LMS of the laser was manipulated by changing the phase-matching temperature of the nonlinear LBO crystal which directly decided the value of the intra-cavity nonlinear loss. The nonlinear loss could be simply marked by the nonlinear conversion efficiency (NCE) η which was defined by the ratio between the power of 532 nm laser and that of the intra-cavity 1064 nm laser. The values of η as a function of the temperature of the LBO crystal and the corresponding LMS were shown in Fig. 4(A) and Fig. 4(B), respectively. When the NCE $\eta \geq 0.28\%$, the laser can work with single-longitudinal mode (SLM) operation as shown in (b_1) of Fig. 4(B), where the nonlinear loss was high enough to suppress the oscillation of non-lasing mode. However, once

Optics EXPRESS

the temperature of the LBO crystal was detuned more than 2 °C ($\eta < 0.28\%$), the laser started to work in multi-longitudinal-mode (MLM) region. At this moment, the nonlinear loss supplied by the nonlinear conversion process was too low to suppress the oscillation of the non-lasing mode. The curve (b_2) of Fig. 4(B) showed the initial LMS of the laser when the NCE $\eta = 0.21\%$, where another two side longitudinal-modes with low intensity appeared and oscillated together with the dominant mode. Through the long-term observation, however, the LMS of the laser as shown in curve (b_2) of Fig. 4(B) gradually evolved into the curve (b_3) of Fig. 4(B). With decreasing NCE η to 0.16%, the intensity of the side modes rapidly increased and mode-hopping phenomenon occurred, and the LMS of the laser rapidly alternated between the curve (b_3) and curve (b_4) of Fig. 4(B). When the NCE was further decreased to $\eta = 0.028\%$, the LMS of the laser was always like curve (b_4) of Fig. 4(B), where it was difficult to distinguish the dominant and side modes because of the strong intensity fluctuation of all the modes. When the NCE η was decreased to zero, the LMS of the laser randomly switched between that of (b_1), (b_2), and (b_3) shown in Fig. 4(B) in a long operating time. We summarized the relationship between the LMS of the laser and the intra-cavity NCE η. When the intra-cavity NCE η was high enough to suppress the oscillation of the non-lasing mode, introducing a nonlinear loss to the laser resonator was a great way to achieve the SLM operation of the laser. However, if the intra-cavity NCE η was too low to suppress the oscillation of the non-lasing mode, the laser run with the MLM operation and intra-cavity nonlinear conversion process could directly induce the strong coupling between different longitudinal-modes. As a result, the frequent and strong mode-hopping appeared.

While the LMS of the laser was monitored, the RIN spectrum of the laser was simultaneously measured corresponding to the different intra-cavity NCE η in the experiment. In the process of the RIN spectrum measurements, the resolution bandwidth and the video bandwidth of the spectrum analyzer were set to be 30 kHz and 30 Hz, respectively. Firstly, to calibrate the QNL, two photodiodes of the BHD were simultaneously illuminated with 1 mW 1064 nm laser, respectively. The obtained spectrum V_1 of the subtracted signal was directly characterized as QNL of the 1064 nm laser under the detection power of 2 mW. Then one of the photodiodes was blocked and the other was illuminated with the power of 1 mW. In this case, spectrum V_2 can be read out by the spectrum analyzer. Lastly, the RIN spectrum of the 1064 nm laser was extracted according V_{obs}=V_2-(V_1-3dB) [48]. In addition, the overall measured RIN spectra had been normalized to that with the largest values of NCE η according to the normalized equation [11, 12],

$$V_n = 10\lg[\frac{10^{V_{obs}/10} - 1}{k} + 1], \tag{1}$$

where V_n was the normalized RIN spectrum, k represented the normalizing factor which was obtained with the intra-cavity FW power corresponding to η of (a_1)~(a_9) divided by that with η of (a_1).

Figure 5 firstly displayed the evolution of RIN spectra of the laser in the case that the laser always worked with SLM operation where the NCE η was decreased from 1.01% to 0.28%. When the NCE η was 1.01% and 0.93%, the RRO peak of the laser was completely suppressed according to the RIN spectrum of (a) and (b) in Fig. 5. When the NCE η was decreased to 0.76% (curve (c) of the Fig. 5), the RRO peak began to pop out and the measured frequency and amplitude of the RRO peak were 788.20 kHz and 25.75 dB, respectively. When the NCE η was further decreased to 0.51% (curve (d) of the Fig. 5), the RRO peak of the laser was so dramatic that it was easy to be observed and measured. At that time, the measured frequency and amplitude of the RRO peak were 840.36 kHz and 28.04 dB, respectively. When the NCE η was decreased to 0.28% (curve (e) of the Fig. 5) corresponding to the edge of the SLM region of the laser, the frequency and amplitude of RRO peak were 937.86 kHz and 32.21 dB, respectively. It was clear that the frequency and amplitude of the RRO peak shifted to the high frequencies and increased with the decrease of the NCE η.

Optics EXPRESS

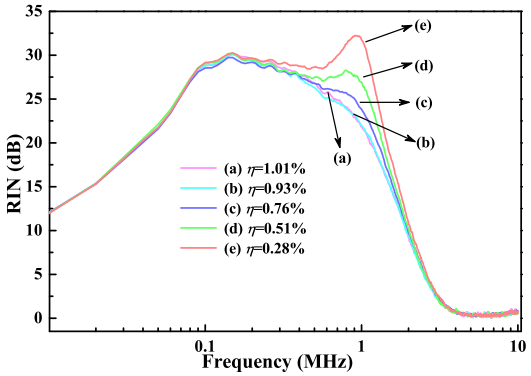

Fig. 5. Measured RIN spectra of the laser worked with SLM operation. Curve (a), the RIN spectrum of the laser with NCE η of 1.01%; curve (b), the RIN spectrum of the laser with NCE η of 0.93%; curve (c), the RIN spectrum of the laser with NCE η of 0.76%; curve (d), the RIN spectrum of the laser with NCE η of 0.51%; curve (e), the RIN spectrum of the laser with NCE η of 0.28%.

The RIN properties of the single-frequency laser with different NCE η can also be well theoretically predicted according to intensity noise spectrum (V_f) of the FW laser [16]

$$V_f = k_1(\omega, \gamma_f)V_{vac1} + k_2(\omega, \gamma_f)V_{vac2} + k_3(\omega_f, \gamma_f)V_p + k_4(\omega_f, \gamma_f)V_{spont} + k_5(\omega_f, \gamma_f)V_{dipole} + k_6(\omega_f, \gamma_f)V_{losses}, \tag{2}$$

where V_{vac1} and V_{vac2} were the vacuum noise caused by the second-harmonic generation and the output coupler, respectively; V_p, V_{spont}, V_{dipole} and V_{losses} were corresponding to the noises coming from the pump source, spontaneous-emission, dipole fluctuation and intra-cavity losses, respectively. The coefficients of $k_1(\omega_f, \gamma_f)$, $k_2(\omega_f, \gamma_f)$, $k_3(\omega_f, \gamma_f)$, $k_4(\omega_f, \gamma_f)$, $k_5(\omega_f, \gamma_f)$ and $k_6(\omega_f, \gamma_f)$ in V_f were the function of ω_f and γ_f.

The frequency of the RRO ω_f and the damping rate of the oscillation γ_f were given by

$$\omega_f = \sqrt{2\kappa_m(G\alpha^2 + \Gamma + \gamma_t) + 2G\alpha^2\kappa_t}, \tag{3}$$

and

$$\gamma_f = 2\kappa_m + G\alpha^2 + \Gamma + \gamma_t. \tag{4}$$

where $2\kappa_m$ was the photon decay rate induced by the output losses; G was the stimulated-emission rate per photon; Γ was the pump rate; γ_t was the atomic spontaneous emission rate from upper level to lower level; $2\kappa_t$ was the total photon decay rate, which was expressed by $2\kappa_t = 2\kappa_m + 2\kappa_l + 2\kappa_n$, where $2\kappa_l$ was the photon decay rate induced by the intra-cavity losses, $2\kappa_n$ was the photon decay rate induced by the nonlinear loss, which was expressed by $2\kappa_n = 2\mu\alpha^2$, μ and α^2 were the nonlinear conversion rate and the intra-cavity photon number, respectively.

According to the equations (2)-(4), the evolution trends of the amplitude and the frequency of the RRO were obtained with the variation of the NCE η, which was completely consistent with the law presented in our previous work [16]. The measured results once again verified that the nonlinear conversion process can modify the laser dynamics and manipulate the RIN of the laser.

However, the stable evolution law of the RIN spectra of the laser did not continue when the NCE η was decreased to 0.21%, where the nonlinear loss is too low to suppress the oscillation of the non-lasing mode. As a result, the side mode began to oscillate together with the dominant oscillating mode and the laser began to work with MLM operation. Figure. 6 recorded the RIN spectra of the FW laser at different instants of time when the NCE η was equal to 0.21%. At the

Optics EXPRESS

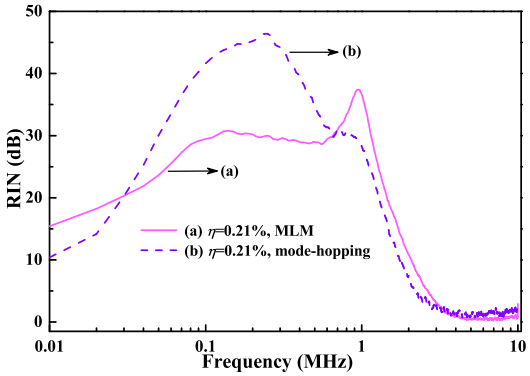

Fig. 6. Measured RIN spectra of the laser with NCE η of 0.21%. Curve (a), the RIN spectrum of the laser worked in MLM; curve (b), the RIN spectrum of the laser worked with mode-hopping.

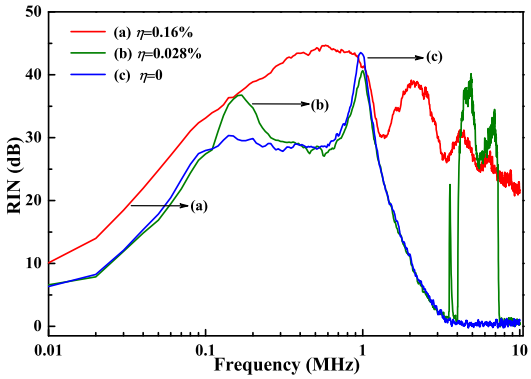

Fig. 7. Measured RIN spectra of the laser worked with MLM operation. Curve (a), the RIN spectrum of the laser with NCE η of 0.16%; curve (b), the RIN spectrum of the laser with NCE η of 0.028%; curve (c), the RIN spectrum of the laser without NCE.

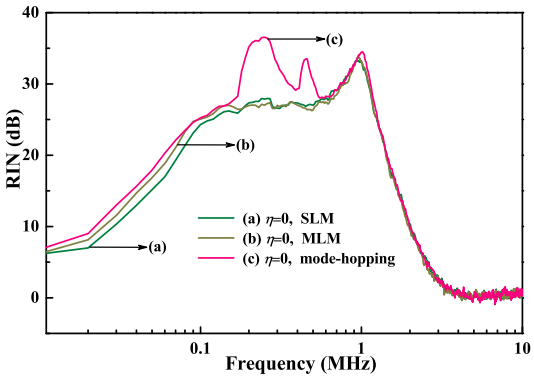

Fig. 8. Measured RIN spectra of the laser without NCE. Curve (a), the RIN spectrum of the laser worked in SLM; curve (b), the RIN spectrum of the laser worked in MLM; curve (c), the RIN spectrum of the laser worked with mode-hopping.

Optics EXPRESS

beginning of the appearance of the side modes (LMS of the laser was like curve (b_2) in (B) of Fig. 4), the intensity of the side modes was small and could be ignored, so the measured RIN spectrum of the FW laser was relatively stable as shown in curve (a) of Fig. 6. With the increase of the intensity and number of the side mode (LMS of the laser was like curve (b_3) in (B) of Fig. 4), the measured RIN spectrum of the FW laser became instable, which was depicted in curve (b) of Fig. 6. The measured results shown in Fig. 6 illustrated that the RIN spectrum of the laser was directly decided by the LMS of the laser. In order to verify the relationship between the RIN spectrum and the LMS of the laser, the RIN spectra of the laser were also measured when the NCE η were separately 0.16%, 0.028% and 0, and the measured results were shown in Fig. 7. Not only NCE η was equal to 0.16% but also 0.028%, the LMS of the laser was both unstable as shown in curve (b_4) in (B) of Fig. 4. In that case, the strong intensity fluctuation of the overall longitudinal-modes and frequent mode-hopping occurred and the measured RIN spectra of the laser were displayed in curve (a) and (b) of Fig. 7. It was clear that the RIN spectrum of the laser strongly fluctuated at low frequencies as well as the high frequencies. However, when the NCE η was decreased to zero, the stable RIN spectrum of the laser was observed once again, which was depicted in curve (c) of Fig. 7. However, the stable RIN spectrum was temporary because the LMS of the laser randomly switched between SLM, MLM and mode-hopping when the NCE η was zero. In consequence, the unstable RIN spectra of the FW laser were observed once more at different instants of time, which were depicted in Fig. 8. The curve (a), (b) and (c) in Fig. 8 were corresponding to the SLM, MLM and mode-hopping, respectively. It was clear that the RIN increase of the laser occurred only at the low frequencies when the NCE η was equal to zero. Compared Fig. 7 to Fig. 8, it was revealed that when the nonlinear loss existed but too low to suppress the oscillation of the non-lasing modes, the different longitudinal modes could strongly couple between each other through the nonlinear process (which was named "green problem" [51, 52]) so that the RIN spectrum of the FW laser strongly fluctuated not only at low frequencies but also high frequencies. In stark contrast, the RIN spectrum fluctuation of the FW laser was observed only at low frequencies when the NCE η was moved away. The measured results also revealed that the RIN spectrum of a high power single-frequency laser with free MLM and mode-hopping was as stable as that of a low power single frequency laser which was often used as the seed source for implementing the injection-locking amplification. It was further verified that introducing large enough nonlinear loss to a resonator was a good way to effectively suppress the MLM and mode-hopping as well as achieve SLM operation of a high power laser.

4. Conclusion

In summary, we firstly constructed a highly stable, low intensity noise all-solid-state single-frequency 1064 nm laser with output power of 50.3 W and perfect beam quality as well as high degree of polarization. Then the influence of LMS of the laser on the laser RIN property was experimentally investigated. The LMS of the laser was manipulated by controlling the temperature of the nonlinear crystal LBO deliberately introduced to the resonator. When the laser worked with SLM operation, the stable RIN spectrum was observed and measured. Moreover, with the decrease of the NCE η, the frequency and amplitude of the RRO peak regularly shifted to the higher frequencies and increased, respectively. The contribution was ascribed to the enough large NCE η which can effectively suppress the oscillating of the non-lasing modes. However, with further decrease of the NCE η, the laser began to work with the MLM or mode-hopping operation and the unstable RIN spectrum of the laser was observed. Once the MLM or mode-hopping phenomenon occurred in the laser, the strong intensity fluctuations would appear not only at low frequencies but also at high frequencies. The reason was ascribed to the coupling of different longitudinal-modes through the nonlinear process. Once the NCE η was moved away, the MLM or mode-hopping can only enhance the fluctuation of the laser RIN spectrum at the low frequencies (lower than the frequency of RRO). Our work essentially provided an important reference for

Optics EXPRESS

the influence of LMS on the RIN properties of a high power laser, which revealed that the key to achieve a stable high power laser with low intensity noise was to realize single-frequency operation of the laser with free MLM and mode-hopping.

Funding

Key Project of the Ministry of Science and Technology of China (2017YFB0301403).

References

1. H. J. Kimble, "The quantum internet," Nature **453**, 1023-1030 (2008).
2. P. Kómár, E. M. Kessler, M. Bishof, L. Jiang, A. S. Søensen, J. Ye, and M. D. Lukin, "A quantum network of clocks," Nat. Phys. **10**, 582-587 (2014).
3. D. J. Wineland, and W. M. Itano, "Laser cooling of atoms," Phys. Rev. A **20**, 1521-1540 (1979).
4. LIGO scientific collaboration and Virgo collaboration, "Observation of gravitational waves from a binary black hole merger," Phys. Rev. Lett. **116**, 061102 (2016).
5. K. Somiya, Y. Chen, S. Kawamura, and N. Mio, "Frequency noise and intensity noise of next-generation gravitational-wave detectors with RF/DC readout schemes," Phys. Rev. D **73**, 122005 (2006).
6. M. Steinke, H. Tünnermann, V. Kuhn, T. Theeg, M. Karow, O. Varona, P. Jahn, P. Booker, J. Neumann, P. Weßels, and D. Kracht, "Single-frequency fiber amplifiers for next-generation gravitational wave detectors," IEEE J. Sel. Top. Quantum Electron. **24**, 3100613 (2018).
7. LIGO Scientific Collaboration, "LIGO: the laser interferometer gravitational-wave observatory," Rep. Prog. Phys. **72**, 076901 (2009).
8. S. Schiller, G. Breitenbach, S. F. Pereira, T. Müller, and J. Mlynek, "Quantum statistics of the squeezed vacuum by measurement of the density matrix in the number state representation," Phys. Rev. Lett. **77**, 2933-2936 (1996).
9. H. Vahlbruch, M. Mehmet, K. Danzmann, and R. Schnabe, "Detection of 15 dB squeezed states of light and their application for the absolute calibration of photoelectric quantum efficiency," Phys. Rev. Lett. **117**, 110801 (2016).
10. A. Congar, K. Hussain, C. Pareige, R. Butté, N. Grandjean, P. Besnard, and S. Trebaol, "Impact of mode-hopping noise on InGaN edge emitting laser relative intensity noise properties," IEEE J. Quantum Electron. **54**, 1100107 (2018).
11. T. C. Ralph, C. C. Harb, and H. A. Bachor, "Intensity noise of injection-locked lasers: Quantum theory using a linearized input-output method," Phys. Rev. A **54**, 4359-4369 (1996).
12. C. C. Harb, T. C. Ralph, E. H. Huntington, I. Freitag, D. E. McClelland, and H. A. Bachor, "Intensity-noise properties of injection-locked lasers," Phys. Rev. A **54**, 4370-4382 (1996).
13. C. C. Harb, T. C. Ralph, E. H. Huntington, D. E. McClelland, H. A. Bachor, and I. Freitag, "Intensity-noise dependence of Nd:YAG lasers on their diode-laser pump source," J. Opt. Soc. Am. B **14**, 2936-2945 (1997).
14. H. D. Lu, J. Su, C. D. Xie, and K. C. Peng, "Experimental investigation about influences of longitudinal-mode structure of pumping source on a Ti:sapphire laser," Opt. Express **19**, 1344-1353 (2011).
15. J. Zhang, Y. L. Chen, K. S. Zhang, T. C. Zhang, C. D. Xie, and K. C. Peng, "Investigation of the characteristics of the intensity noise of singly resonant active second-harmonic generation," J. Opt. Soc. Am. B **17**, 1695-1703 (2000).
16. H. D. Lu, Y. R. Guo, and K. C. Peng, "Intensity noise manipulation of a single-frequency laser with high output power by intracavity nonlinear loss," Opt. Lett. **40**, 5196-5199 (2015).
17. T. J. Kane, "Intensity Noise in Diode-Pumped Single-Frequency Nd:YAG Lasers and its Control by Electronic Feedback," IEEE Photon. Technol. Lett. **2**, 244-245 (1990).
18. C. C. Harb, M. B. Gray, H. A. Bachor, R. Schilling, P. Rottengatter, I. Freitag, and H. Welling, "Suppression of the intensity noise in a diode pumped neodymium:YAG nonplanar ring laser," IEEE J. Quantum Electron. **30**, 2907-2913 (1994).
19. B. Willke, S. Brozek, K. Danzmann, V. Quetschke, and S.Gossler, "Frequency stabilization of a monolithic Nd:YAG ring laser by controlling the power of the laser-diode pump source," Opt. Lett. **25**, 1019-1021 (2000).
20. J. Zhang, C. D. Xie, and K. C. Peng, "Electronic feedback control of the intensity noise of a single-frequency intracavity-doubled laser," J. Opt. Soc. Am. B **19**, 1910-1916 (2002).
21. J. Zhang, H. L. Ma, C. D. Xie, and K. C. Peng, "Suppression of intensity noise of a laser-diode-pumped single-frequency Nd:YVO_4 laser by optoelectronic control," Appl. Opt. **42**, 1068-1074 (2003).
22. M. Heurs, V. M. Quetschke, B. Willke, K. Danzmann, and I. Freitag, "Simultaneously suppressing frequency and intensity noise in a Nd:YAG nonplanar ring oscillator by means of the current-lock technique," Opt. Lett. **29**, 2148-2150 (2004).
23. M. Heurs, U. T. Meier, V. M. Quetschke, B. Willke, I. Freitag, and K. Danzmann, "Intensity and frequency noise reduction of a Nd:YAG NPRO via pump light stabilisation," Appl. Phys. B **85**, 79-84 (2006).
24. A. E. Amili, and M. Alouini, "Noise reduction in solid-state lasers using a SHG-based buffer reservoir," Opt. Lett. **40**, 1149-1152 (2015).
25. K. Audo, and M. Alouini, "Intensity noise cancellation in solid-state laser at 1.5 μm using SHG depletion as a buffer reservoir," Appl. Opt. **57**, 1524-1529 (2018).

Optics EXPRESS

26. B. Willke, N. Uehara, E. K. Gustafson, R. L. Byer, P. J. King, S. U. Seel, and R. L. Savage, "Spatial and temporal filtering of a 10-W Nd:YAG laser with a Fabry–Perot ring-cavity premode cleaner," Opt. Lett. **23**, 1704-1706 (1998).
27. W. M. Tulloch, T. S. Rutherford, E. H. Huntington, R. Ewart, C. C. Harb, B. Willke, E. K. Gustafson, M. M. Fejer, R. L. Byer, S. Rowan and J. Hough, "Quantum noise in a continuous-wave laser-diode-pumped Nd:YAG linear optical amplifier," Opt. Lett. **23**, 1852-1854 (1998).
28. Y. L. Chen, J. Zhang, Y. M. Li, K. S. Zhang, C. D. Xie, and K. C. Peng, "Reduction of intensity noise of single-frequency Nd:YVO_4 laser using mode cleaner," Chin. J. Lasers **28**, 197-200 (2001).
29. C. D. Nabors, A. D. Farinas, T. Day, S. T. Yang, E. K. Gustafson, and R. L. Byer, "Injection locking of a 13-W cw Nd:YAG ring laser," Opt. Lett. **14**, 1189-1191 (1989).
30. I. Freitag, D. Golla, S. Knoke, W. Schöne, H. Zellmer, A. Tünnermann, and H. Welling, "Amplitude and frequency stability of a diode-pumped Nd:YAG laser operating at a single-frequency continuous-wave output power of 20 W," Opt. Lett. **20**, 462-464 (1995).
31. R. L. Savage-Jr, P. J. King, and S. U. Seel, "A highly stabilized 10-watt Nd:YAG laser for the laser interferometer gravitational-wave observatory (LIGO)," Laser Phys. **8**, 679-685 (1998).
32. D. J. Ottaway, P. J. Veitch, C. Hollitt, D. Mudge, M. W. Hamilton, and J. Munch, "Frequency and intensity noise of an injection-locked Nd:YAG ring laser," Appl. Phys. B **71**, 163-168 (2000).
33. K. Takeno, T. Ozeki, S. Moriwaki, and N. Mio, "100 W, single-frequency operation of an injection-locked Nd:YAG laser," Opt. Lett. **30**, 2110-2112 (2005).
34. B. Willke, K. Danzmann, M. Frede, P. King, D. Kracht, P. Kwee, O. Puncken, R.L. Savage Jr., B. Schulz, F. Seifert, C. Veltkamp, S. Wagner, P. Wessels, and L. Winkelmann, "Stabilized lasers for advanced gravitational wave detectors," Class. Quantum Grav. **25**, 114040 (2008).
35. L. Winkelmann, O. Puncken, R. Kluzik, C. Veltkamp, P. Kwee, J. Poeld, C. Bogan, B. Willke, M. Frede, J. Neumann, P. Wessels, and D. Kracht, "Injection-locked single-frequency laser with an output power of 220 W," Appl. Phys. B **102**, 529-538 (2011).
36. P. Kwee, C. Bogan, K. Danzmann, M. Frede, H. Kim, P. King, J. Pöld, O. Puncken, R. L. Savage, F. Seifert, P. Wessels, L. Winkelmann, and B. Willke, "Stabilized high-power laser system for the gravitational wave detector advanced LIGO," Opt. Express **20**, 10617-10634 (2012).
37. N. B. Abraham, J. C. Huang, D. A. Kranz, and E. B. Rockower, "Amplified-spontaneous-emission intensity fluctuations," Phys. Rev. A **24**, 2556-2566 (1981).
38. L. McDonagh, R. Wallenstein, R. Knappe, and A. Nebel, "High-efficiency 60 W TEM_{00} Nd:YVO_4 oscillator pumped at 888 nm," Opt. Lett. **31**, 3297-3299 (2006).
39. L. McDonagh, and R. Wallenstein, "Low-noise 62 W CW intracavity-doubled TEM_{00} Nd:YVO_4 green laser pumped at 888 nm," Opt. Lett. **32**, 802-804 (2007).
40. L. McDonagh, R. Wallenstein, and A. Nebel, "111W, 110 MHz repetition-rate, passively mode-locked TEM_{00} Nd:YVO_4 master oscillator power amplifier pumped at 888 nm," Opt. Lett. **32**, 1259-1261 (2007).
41. Y. J. Wang, Y. H. Zheng, Z. Shi, and K. C. Peng, "High-power single-frequency Nd:YVO_4 green laser by self-compensation of astigmatisms," Laser Phys. Lett. **9**, 506-510 (2012).
42. Y. H. Zheng, F. Q. Li, Y. J. Wang, K. S. Zhang, K. C. Peng, "High-stability single-frequency green laser with a wedge Nd:YVO_4 as a polarizing beam splitter," Opt. Commun. **283**, 309-312 (2010).
43. J. Q. Zhao, Y. Z. Wang, B. Q. Yao, and Y. L. Ju, "High efficiency, single-frequency continuous wave Nd:YVO_4/YVO_4 ring laser," Laser Phys. Lett. **7**, 135-138 (2010).
44. Y. H. Zheng, and K. S. Zhang, "All-solid-state blue laser of single-frequency operation end-pumped by diode laser," Acta Sinica Quantum Optica **10**, 42-46 (2004).
45. K. Kato, "Temperature-tuned 90° phase matching properties of LBO," IEEE J. Quantum Electron. **30**, 2950-2952 (1994).
46. H. D. Lu, J. Su, Y. H. Zheng, and K. C. Peng, "Physical conditions of single-longitudinal-mode operation for high-power all-solid-state lasers," Opt. Lett. **39**, 1117-1120 (2014).
47. H. D. Lu and K. C. Peng, "Realization of the single-frequency and high power as well as frequency-tuning of the laser by manipulating the nonlinear loss," J. Quantum Opt. **21**, 171-176 (2015).
48. X. L. Jin, J. Su, Y. H. Zheng, C. Y. Chen, W. Z. Wang, and K. C. Peng, "Balanced homodyne detection with high common mode rejection ratio based on parameter compensation of two arbitrary photodiodes," Opt. Express **23**, 23859-23866 (2015).
49. Y. R. Guo, H. D. Lu, Q. W. Yin, and J. Su, "Intra-cavity round-trip loss measurement of all-solid-state single-frequency laser by introducing extra nonlinear loss," Chin. Opt. Lett. **15**, 021402 (2017).
50. T. Okoshi, K. Kikuchi, and A. Nakayama, "Novel method for high resolution measurement of laser output spectrum," Electron. Lett. **16**, 630-631 (1980).
51. T. Baer, "Large-amplitude fluctuations due to longitudinal mode coupling in diode-pumped intracaviy-doubled Nd:YAG lasers," J. Opt. Soc. Am. B **3**, 1175-1180 (1986).
52. K. I. Martin, W. A. Clarkson, and D. C. Hanna, "Self-suppression of axial mode hopping by intracavity second-harmonic generation," Opt. Lett. **22**, 375-377 (1997).